Analysis and Design of Asymmetric Oscillation for Caterpillar-like Locomotion

Guoyuan Li[1], Wei Li[1], Jianwei Zhang[2] and Houxiang Zhang[1]

1. Faculty of *Maritime Technology and Operations, Aalesund University College*, *Aalesund, 6009*, *Norway*

2. *Department of Computer Science, University of Hamburg, Hamburg, 22527 Germany*

+47-10-70161325, guli@hials.no

Abstract

Caterpillar crawling is distinct from that of other limbless animals. It is simple but efficient. This paper presents a novel mechanism to duplicate the movement to a modular caterpillar-like robot. First, how caterpillars move in nature is investigated and analyzed systematically. Two key locomotive properties are abstracted from the body shape of caterpillars during crawling. Then, based on a morphological mapping, a hypothesis of asymmetric oscillation with a ratio of two is proposed, followed by a thorough analysis of the kinematics of the caterpillar-like robot. The asymmetric oscillating mechanism is proved capable of generating stable caterpillar-like locomotion. Next, taking advantage of the two locomotive properties and the hypothesis, a new central pattern generator (CPG) model is designed as the controller of the robot. The model can not only generate the signal as expected, but also provide explicit control parameters for online modulation. Finally, simulation and on-site experiments are carried out. The results confirm that the proposed method is effective for caterpillar-like locomotion.

Keywords: asymmetric oscillation; kinematic analysis; central pattern generator; caterpillar-like locomotion

1 Introduction

Limbless animals comprise one of the main branches in the animal kingdom. Driven by the instinct for hunger or mating, they have evolved a variety of limbless locomotion capabilities, such as serpentine creeping, peristaltic crawling, and anguilliform swimming. Limbless locomotion is more stable than other forms of locomotion since animals that use it have a low center of mass and a large contact area that prevent them from falling over. To move from one place to another in an efficient manner, they propagate flexural traveling waves along their body length, so that the force generated between the body and the surrounding environment propels them forward. In essence, they move by specific patterns of body coordination and muscle contraction and relaxation [1].

Motivated by the advantages of limbless locomotion in animals, researchers have been interested in replicating these movements under physically modeled limbless robots for years. A diversity of limbless robots have been developed, including snake-like robots [2], worm-like robots [3], caterpillar-like robots [4], and fish-like robots [5]. The limbless design offers significant benefits for dealing with complex environments that traditional robots with appendages such as wheels or legs fail to traverse.

How a limbless robot moves depends on the robot's configuration, as well as auxiliary equipment. There are several types of limbless locomotive modes in the literature [6]. First, limbless robots without any auxiliary equipment can generate locomotion by coordinating all the modules in a special temporal sequence. The purpose of the pure body undulation is to employ traveling body waves for propulsion. Some modular robots, such as the Polyboy robot [7] and the M-TRAN robot [8], belong to this category. Second, limbless robots with shrinkable modules can perform rectilinear motion that is typically used by large snakes like pythons. For example, the Crystalline robot, whose modules can be extended to twice its original length, achieves the movement by extending and compressing each module in turn from tail to head [9]. Third, passive wheels can be placed on the underside along the body length of a limbless robot. The passive wheels can increase frictional force in the lateral direction but reduce the resistance in the forward direction. Limbless robots with passive wheels can perform smooth lateral undulation on flat terrains. This locomotive mode has been verified on different robot prototypes, such as the ACM

III robot [10] and the Amphibot I robot [11]. Fourth, limbless robots are able to be equipped with active wheels/treads. Powered wheels/treads provide these robots with higher flexibility in complex environments. Limbless robots do not have to use body undulation but utilize the propulsion of the wheels/treads to traverse obstacles. The representatives of this locomotive mode include the ACM R4 robot [12] and the OT-4 robot [13].

Biologists have also long been interested in the principles of animal locomotion at the neural level. Neurobiological studies have shown that rhythmic movements are generated in the spinal cord by a group of neural networks called central pattern generators (CPGs) [14]. CPG can not only produce rhythmic signals that control muscular activity to generate rhythmic patterns, but also have the ability to produce sensory feedback integration to alter the pattern of locomotion, which helps animals to adapt to their surroundings during locomotion. Although the underlying mechanisms of CPG are not yet fully understood, the concept has been accepted and applied in the robotics domain. CPG is considered an elegant solution for online gait generation [15]. Compared to traditional methods, such as numerical techniques, geometric methods, and intelligent control techniques, CPG-based control has many appealing properties, including the ability to deal with redundancies, to recover from perturbations, and to integrate sensory feedback as well as online modulation.

Our research aims to develop a hierarchical control system for caterpillar-like robots, including a CPG model containing a reflex mechanism as well as biological features and learning algorithms for sensor-servo-based behavior control and active perception of the environment to complete the system. Although caterpillar-like locomotion has been implemented by using the analytical method [16] and the gait control table method [17], these designs only focus on the specific body shape; how to abstract the movement from nature was not addressed. Furthermore, considering that the caterpillar locomotion is very different from the locomotion of snakes, worms, and fishes, the existing CPG models are not suitable to be directly applied on caterpillar-like robots. The research presented in this paper focuses on the analysis and the design of the CPG model for caterpillar-like locomotion. It builds upon the work presented in [18] by adding a thorough analysis and evaluation. The contribution of this paper is twofold. First, a new CPG model based on a Hopf oscillator is proposed, with an emphasis on the gait analysis under the

asymmetric oscillation. Second, the feasibility and effectiveness of the proposed approach are verified through simulation and real on-site experiments.

2 Inspiration from caterpillars

This section presents how caterpillars crawl in complicated environments and identifies their locomotion properties. It also presents a mapping from caterpillars to caterpillar-like robots to simplify the description of further locomotion analysis.

2.1 Caterpillar locomotion properties

In nature, caterpillars are able to perform three types of gaits: forward moving, reverse moving, and rolling [19, 20]. In most cases, caterpillars use forward moving for locomotion at only 10% of the maximum speed. Forward moving is produced by a series of contraction and relaxation of body waves, as shown in Fig. 1. A step cycle begins with lifting up the terminal proleg (TP). The TP moves forward and anchors one step ahead, forming a characteristic traveling 'hump' on the back of the caterpillar. Here, we call the 'hump' – a 'half wave'. Once the TP is set, the half wave propagates along the body forward from tail to head. Segments in the half wave are raised up from and later lowered back to the ground, one after another. The half wave disappears until the head segment attaches to the ground. Thus, the step cycle is completed.

Trimmer et al. has separated the forward locomotion of caterpillars from that of worms and other mollusks [21, 22]. One key difference is that the segments in caterpillars are not always movable. For each segment, a swing phase and a stance phase appear alternately during the stepping pattern. Brackenbury has observed that each segment of caterpillars with a duty factor of 35% in the stance phase can maximize stability [20]. In contrast to other limbless animals, the two phases allow caterpillars to climb more stably because most of their body attaches to the substrate. Another interesting property for caterpillar forward locomotion is the phase lag in sequential segments. The half wave propagates forward with a phase difference of 30-35° between the mid-abdominal segments. In light of the two properties, a novel CPG model producing asymmetric oscillation is designed, which will be introduced in detail in Section 4.

2.2 Morphological mapping

In robotics, a challenge of caterpillar-like robots is how to reproduce caterpillars using soft materials. Caterpillars have a soft-body structure without a skeleton. They can bend and twist in a

multidimensional workspace. Using soft materials provides the most flexibility for the robot. Although there are a few attempts to build soft-bodied robots for deformation and locomotion, most of them can only function in a specific environment [23].

An alternative is to use rigid elements. In fact, the morphology of caterpillars is chain-type with a high degree of modularity. Each segment in caterpillars contains about 70 muscles and each muscle is actuated by one motoneuron [21]. Consequently, caterpillar locomotion is mainly controlled by only a few hundred motoneurons. From an abstract viewpoint, caterpillars have a heterogeneous morphology with different sizes of segments. An intuitive way to imitate caterpillars is to replace these segments with modules and joints, as shown in Fig. 2. However, for simplicity, the modules are supposed to be identical in both size and weight. In order to analyze the kinematics of caterpillars, a skeleton model is employed here to represent the segment of the caterpillar-like robot. We assume that a positive angle is generated if the right side of a module bends upwards with respect to the left side of the module, while a negative angle is produced if it bends downwards.

3 Caterpillar-like locomotion analysis

In this section, we analyze the kinematics of caterpillar-like robots. The changes in the half wave generated during the locomotion, including body shape, joint variation, collision and displacement, are thoroughly analyzed.

3.1 Body shape analysis

We first study the discrete body shapes in the half wave. Assume the body shape is symmetric. According to the number of involved modules in the half wave, there are two types of body shapes, as shown in Fig. 3a. Considering the symmetry, the module in the middle of the body arc bends oppositely twice as much as the modules at both ends. From Fig. 3a, it is noted that if a phase lag exists between these involved modules, the corresponding joint variation over discrete time must be asymmetric, with a ratio of 2. Fig. 3b depicts how a half wave is generated and propagated forward over a discrete time sequence if the phase lag is locked and an asymmetric oscillating ratio of 2 is reached. The diagram on the left of Fig. 4 summarizes the angle variation during the swing phase: (1) the curve should be enclosed and separated into three regions; (2) the three regions have the same time span; and (3) the sum of the enclosed area equals 0.

For continuous oscillation, a hypothesis of using sinusoidal function while satisfying the above conditions is proposed, as shown in the diagram on the right of Fig. 4. The formation of the curve can be described as:

$$\alpha_i = A \cdot \mathrm{sgn}(t) \cdot \sin(\omega t + i\phi)$$
$$\mathrm{sgn}(t) = \begin{cases} 1 & if \ \sin(\omega t + i\phi) \geq 0 \\ 2 & otherwise \end{cases} \quad (1)$$

where A is the oscillation amplitude; ω is the frequency; and ϕ is the phase difference. Similar to the discrete time sequence, the angle variation in the swing phase is asymmetric and lasts three identical sections of time span, i.e., a period of $3\pi/\omega$. The following sections will analyze and prove the proposed asymmetric oscillation is stable for caterpillar-like locomotion.

3.2 Joint analysis

Assume the caterpillar-like robot has enough modules to form the half wave. The fundamental requirement for caterpillar-like locomotion is that during the propagation of the half wave, both ends of the robot should be parallel to the ground to make the movement stable. Fig. 5a illustrates that the angle at both ends is determined by the sum of joint angle of each module in the half wave. If the phase difference ϕ is chosen as:

$$\phi = \frac{\pi}{n}, \quad (n \in N, \ n \geq 2) \quad (2)$$

the fundamental requirement is satisfied, i.e., the sum of the angles in the half wave is equal to 0.

Proof.

Since the module angle in the stance phase is always 0, only the modules in the swing phase are considered. From the right diagram in Fig. 4, the asymmetric oscillation lasts a phase of 3π. Let m be the number of involved modules in the swing phase. Then we get:

$$m = \left\lfloor \frac{3\pi}{\phi} \right\rfloor \quad (3)$$

There are two cases that occur alternatively in the swing phase, both of which will be proven to satisfy the fundamental requirement.

Case 1: $\omega t = k\pi$ ($k \in N$)

In this case, the phase of the m modules will be uniformly distributed in a phase of 3π. From (1) and (2), α_0 and α_{3n} are both 0. Thus the number of involved modules is:

$$m = \left\lfloor \frac{3\pi}{\phi} \right\rfloor = 3n-1, \quad (n \in N,\ n \geq 2) \tag{4}$$

The sum of the angles would be:

$$\sum_{i=1}^{3n-1} \alpha_i = \sum_{i=1}^{n-1} (\alpha_i + \alpha_{i+n} + \alpha_{i+2n}) + \alpha_n + \alpha_{2n} \tag{5}$$

The result follows by combining (1), (2) with (5):

$$\begin{aligned} \sum_{i=1}^{3n-1} \alpha_i &= \sum_{i=1}^{n-1} (A \cdot \sin(i\phi) + 2A \cdot \sin((i+n)\phi) + A \cdot \sin((i+2n)\phi)) \\ &= 0 \end{aligned}$$

Case 2: $\omega t \neq k\pi$ ($k \in N$)

This case happens when the phase of each module is within the intervals of one phase difference:

$$\begin{aligned} & i\phi < \omega t + i\phi < (i+1)\phi \\ & \Rightarrow 0 < \omega t < \phi \end{aligned} \tag{6}$$

First we prove that in every phase of π, there are *n* oscillators involved. Suppose without loss of generality that there are *n'* oscillators in phase [*0, π*]. Then the phase of the *n'*th oscillator satisfies:

$$\pi - \phi < \omega t + (n'-1)\phi < \pi \tag{7}$$

Combining (2), (6) with (7), we get

$$n' = n \tag{8}$$

It is true that the same results are obtained in the phase of [*π, 2π*] and [*2π, 3π*]. However, we omit these details here since the proving process is similar to the one aforementioned. Then the number of modules in the swing phase is

$$m = 3n' = 3n, \quad (n \in N,\ n \geq 2) \tag{9}$$

Thus, the sum of angles in the swing phase can be calculated as follows:

$$\begin{aligned} \sum_{i=0}^{3n-1} \alpha_i &= \sum_{i=0}^{n-1} (A \cdot \sin(\omega t + i\phi) + 2A \cdot \sin(\omega t + (i+n)\phi) \\ &\quad + A \cdot \sin(\omega t + (i+2n)\phi)) \\ &= 0 \end{aligned}$$

where the last equality follows from (1) and (2). That completes the proof.

The result indicates that the generated half wave provides a basic stability for both ends of the robot parallel to the ground during the caterpillar-like locomotion.

3.3 Collision analysis

From (1) and (2), the amplitude *A* and the phase difference ϕ affect the body arc in the half wave simultaneously. A body collision may occur if the two parameters are not adequately taken into account. Fig. 5b illustrates a body collision caused by increasing the amplitude *A*. It is found

that if the sum of consequent positive angles in the half wave exceeds 90°, a collision will occur in the body arc. To avoid such a circumstance, a constraint between the two parameters must meet:

$$\sum_{i=0}^{\lfloor \frac{m}{3} \rfloor} \alpha_i < \frac{\pi}{2} \tag{10}$$

We prove that if the amplitude A and the phase difference ϕ are set:

$$A < \frac{\pi}{2} \cdot \sin(\frac{\phi}{2}) \tag{11}$$

the constraint in (10) will be also satisfied.

Lemma

$$\sum_{i=0}^{N} \sin(x + i\phi) = \frac{\sin(x + \frac{N\phi}{2}) \cdot \sin(\frac{N+1}{2}\phi)}{\sin(\frac{\phi}{2})} \quad (\phi \neq 2k\pi)$$

Proof.

Let $S = \sum_{i=0}^{N} \sin(x + i\phi)$, then we get

$$\begin{aligned} \cos(\phi) \cdot S &= \cos(\phi) \cdot (\sin x + \sin(x+\phi) ... + \sin(x + N\phi)) \\ &= \frac{1}{2}[2S + \sin(x + (N+1)\phi) + \sin(x - \phi) \\ &\quad - \sin x - \sin(x + N\phi)] \end{aligned}$$

by the product-to-sum formulas, and the sum is immediate

$$S = \frac{\sin(x + (N+1)\phi) + \sin(x - \phi) - \sin x - \sin(x + N\phi)}{2(\cos(\phi) - 1)}$$

Thus the result follows by using the sum-to-product formulas.

Now we prove

$$\sum_{i=0}^{\lfloor \frac{m}{3} \rfloor} \alpha_i < A / \sin(\frac{\phi}{2}) \tag{12}$$

Proof.

As proved in Section 3.2, one third of the modules' phases are located in [*0, π*]. According to the Lemma, the sum of their angles should be:

$$\sum_{i=0}^{\lfloor \frac{m}{3} \rfloor} \alpha_i = A \cdot \frac{\sin(\frac{n\phi}{2}) \cdot \sin(\omega t + \frac{n-1}{2}\phi)}{\sin(\frac{\phi}{2})} \tag{13}$$

Note that the phase of *n*th module should be in the range

$$\pi - \phi \leq \omega t + (n-1)\phi \leq \pi \tag{14}$$

Substituting (2) into (14) yields

$$\begin{aligned} &\frac{\pi}{2}-\frac{\phi}{2} \le \omega t + \frac{n-1}{2}\phi \le \frac{\pi}{2}+\frac{\phi}{2} \\ &\Rightarrow \sin(\omega t + \frac{n-1}{2}\phi) \le 1 \end{aligned} \tag{15}$$

Eq. (12) is obtained by combining (13), (15) with (2). Thus, according to (12), Eq. (10) is satisfied once (11) is set. That completes the proof.

From the result, it is worth noting that once the phase difference ϕ is set, the maximum acceptable amplitude A can be determined.

3.4 Vertical displacement analysis

From the point of view of locomotion, the stability of caterpillar-like locomotion relies on not only the sum angles in the half wave, but also the vertical displacement between both ends of the robot, as shown in Fig. 5c. Here, we use the kinematic method to analyze the vertical displacement at both ends. Let the left end of the robot be the origin and $P_i = [x_i\ y_i]^T$ be the position of the ith module from the origin. Then, all the module positions can be calculated in an iterative manner:

$$\begin{cases} p_0 = \left[\frac{L}{2}\ \ 0\right]^T \\ p_{i+1} = p_i + R_i \cdot [L\ \ 0]^T \end{cases} \tag{16}$$

where L is the module length, and R is the rotation matrix which is given by

$$R_i = \begin{bmatrix} \cos(\sum_{j=0}^{i}\alpha_j) & -\sin(\sum_{j=0}^{i}\alpha_j) \\ \sin(\sum_{j=0}^{i}\alpha_j) & \cos(\sum_{j=0}^{i}\alpha_j) \end{bmatrix} \tag{17}$$

The vertical displacement between the two ends of the robot is a function of angles by the m modules involved in the half wave:

$$\Delta y = y_m = L \cdot \sum_{i=0}^{m-1} \sin(\sum_{j=0}^{i}\alpha_j) \tag{18}$$

Fig. 6 shows how the maximum vertical displacement varies with the amplitude and the phase difference in a one-step cycle. The module length L is set to be equal to the length of a real module (*76mm*). Collision avoidance among modules is taken into consideration, where a collision area is set up according to the constraint in (11). Note that when the phase difference satisfies (2), there is almost no vertical displacement at both ends of the robot.

This result shows that the caterpillar-like locomotion is stable, as both ends of the robot can be placed in parallel during the locomotion, and be kept in the same plane as well.

3.5 Horizontal displacement analysis

According to equation (16) and (17), the position of modules in the half wave can be calculated iteratively. Fig. 7a illustrates how the body arcs change with respect to different phase differences. Note their amplitudes are set at either $45°$ or the maximum acceptable amplitude according to (11). From the figure, the horizontal length of the body arc increases with the decrease of the phase difference. This is because the increased number of involved modules contributes partially to the horizontal length.

To analyze the horizontal length qualitatively, we define the horizontal displacement per step cycle as the difference between the length of the modules involved in the body wave and the horizontal length of the corresponding body arc:

$$\Delta\lambda = L \cdot (m - \sum_{i=0}^{m-1} \cos(\sum_{j=0}^{i} \alpha_j)) \tag{19}$$

Combining with (1), (2), (3) and (11), $\Delta\lambda$ is a function of the amplitude A and the phase difference ϕ, as shown in Fig. 7b. It is found that $\Delta\lambda$ increases with the growth of A, while it decreases with the growth of ϕ. The reasons are twofold. On the one hand, from (1) and (19), increasing A will increase the module angle α and indirectly increase $\Delta\lambda$. On the other hand, according to (3), when ϕ decreases, the involved modules m increase, leading to an increase of $\Delta\lambda$.

4 Design of asymmetric oscillator

This section proposes a CPG-based control system to realize the caterpillar-like locomotion. Suppose a modular caterpillar-like robot with a pitch-pitch connection is constructed as the test bed of our approach. To achieve stable caterpillar-like locomotion, we design a CPG model based on the analysis of the continuous asymmetric oscillation.

Fig. 8 shows the CPG-based control model for the caterpillar-like robot. It consists of two components: the enable signal and the CPG network. The enable signal plays a role in switching module states back and forth between the swing phase and the stance phase. For modules in the stance phase, the enable signal turns off to block CPG outputs from transmitting to the corresponding modules. While for modules in the swing phase, it turns on to release CPG outputs, driving the corresponding modules to form the half wave. A chain topology of oscillators is built to synchronize CPG outputs under a desired phase difference. Each oscillator contains two mutually inhibiting neurons and one motoneuron (M). The two neurons serve as an extensor (e) and a flexor (f). The motoneuron, together with the enable signal, determines the output of the

oscillator. As a consequence, the caterpillar-like locomotion is achieved, taking advantage of the combined effects from the enable signal and the CPG network.

To describe the oscillator model more specifically, we further assign it by function to three individual parts, as shown in Fig. 9. In the "signal generation" part, the extensor and the flexor are designed to provide a self-sustaining mechanism – they are simplified and modeled as Hopf oscillators:

$$\begin{cases} x_i' = \omega y_i + x_i(A^2 - x_i^2 - y_i^2) \\ y_i' = -\omega x_i + C_i \end{cases} \tag{20}$$

where x and y are the state variables for the neuron; ω and A represent the intrinsic frequency and amplitude, respectively; C is the total coupling acting on the neuron. Two types of coupling are employed for phase lag generation. First, the ipsilateral coupling from other connected oscillators guarantees a phase locking phenomenon. Second, the contralateral coupling between the extensor and the flexor enables a fixed phase lag of π, which maintains the two neurons in a steady anti-phase state after some oscillatory cycles. Adapted from [24], the two types of coupling can be described as:

$$C_i = \sum_j \frac{w}{A}(x_j \sin\phi + y_j \cos\phi - y_i) - \frac{w}{A}(y_i + \bar{y}_i) \tag{21}$$

where w is the coupling weight that determines the strength of the coupling; ϕ is the phase difference between the connected oscillators. The overscore of the state variable represents the state of the opposite neuron in the same oscillator.

Once the symmetric signals are generated, the "signal processing" part starts to make trimming and stretching operations. All the negative signals are trimmed before further operations:

$$u_{\{e,f\}i} = \max(x_{\{e,f\}i}, 0) \tag{22}$$

The variable u records the non-negative value of the neuron. Then a stretching operation is applied on the two neurons by multiplying u_e and u_f by two different oscillating weights, m_e and m_f, respectively. After the operations, the signals become multi-segment and asymmetric.

The last step is to integrate the signals into a continuous signal and filter it as needed. Note the processed signal from the flexor is reversed before adding to the motoneuron. Given the fact that the two neurons will oscillate in anti-phase, the motoneuron fully incorporates these two complementary processed signals into a continuous signal. In addition, in order to switch between

the swing phase and the stance phase, an enable signal is applied on the motoneuron:

$$En_i = \begin{cases} 1 & if \quad t_f < t < t_f + 3\pi / \omega \\ 0 & otherwise \end{cases} \tag{23}$$

$$out_i = En_i(m_e u_{ei} - m_f u_{fi}) \tag{24}$$

The enable signal *En* is defined as a piecewise function. It depends on the specific time at which the motoneuron fires. At some instant t_f when the output of the motoneuron *out* crosses a predefined threshold, the corresponding module is enabled and begins to swing for a period of $3\pi/\omega$. After that, the module is disabled as it enters the stance phase. Table 1 summarizes the range of related parameters in the CPG network for achieving stable caterpillar-like locomotion.

5 Simulation and experiments

To validate the effectiveness of the proposed CPG model, caterpillar-like locomotion was first imitated in the Open Dynamic Engine (ODE) software [25], and then implemented on a real robot. Locomotion comparison with real caterpillars and energy efficiency evaluations are also discussed in this section.

5.1 Caterpillar-like locomotion simulation

For simplicity, a caterpillar-like robot was designed as a chained of modules. Each module is a simple rigid box. A one-dimensional joint placed along the horizontal axis between each box-type module allows rotation in a vertical plane with a range of $\pm 90°$.

In order to comply with the rules in the real world, the gravity was set to $-9.81 m/s^2$ and the friction coefficient to *0.6*. The internal states *x* and *y* in each oscillator is initialized to random values around 0. A timer is assigned to each oscillator as the enable signal. The parameters of the CPG network are set $\omega=1.5\pi$, $A=35$, $\varphi=\pi/2$, and $w=2$. Fig. 10 shows the outputs of the CPG model. Different color bars indicate the duration of the swing phase for the corresponding modules. For the sake of concision, only three outputs of the oscillators are shown here. Fig. 11 illustrates a complete process of the one-step cycle of caterpillar-like locomotion. The result shows the simulated caterpillar-like robot performed three similar phases, i.e., construction, propagation, and destruction, as a real caterpillar does during locomotion.

Apart from the locomotion, the modulation of the body shape was also investigated. Taking advantage of online modulation of the CPG model, it is convenient to modify the half wave by

changing the parameters A and ϕ, as shown in Fig. 12. The result is consistent with the analysis in Section 3.5. The body arc involves more modules to generate the half wave if ϕ decreases according to (2). Modifying A has no effect on the number of involved modules, but an effect on the bending of the body arc. In addition, collision happens if A violates the constraint in (11).

The simulation results show the correctness of the theoretical analysis in generating and modulating the half wave.

5.2 Locomotion comparison with real caterpillars

A pitch-pitch connected modular caterpillar-like robot with eight GZ-I modules was constructed as the test bed of this experiment. Table 2 shows the details of the GZ-I module [26]. The robot is controlled by a PC via a cable. The control is open loop with all the desired angles sent to the servo controller with an empirical sampling time period of *80ms*. Fig. 13 shows a series of pictures in a complete step cycle of caterpillar-like locomotion taken from a video recorded for gait analysis, in which the parameters of the CPG network used in the simulation are used. The robot takes about *4.5s* per cycle and achieves a mean forward speed of about *1.4cm/s*. The result shows the caterpillar-like locomotion is demonstrated as stable as the analysis in Section 3.

The difference in the displacement in the horizontal direction between the robot and real caterpillars was studied, as shown in Fig. 14. Both locomotion patterns have obvious swing and stance phases. Without consideration of size difference, they perform similar locomotor curves except the head and the terminal segment. The reason is twofold. First, for real caterpillars, the head moves continuously rather than cyclically [27]. Besides, due to the length difference, the movements of the terminal segment are distinct from those in the mid-body segments [21]. Second, for the robot, all the modules have a unified specification. They move successively in the same pattern. In spite of the slight difference of locomotion pattern between real caterpillars and the robot, the dominant locomotion properties are duplicated for the caterpillar-like locomotion.

In addition to the whole locomotion comparison, data analysis for individual modules was also carried out. In [28], Trimmer et al. has observed the kinematic parameters of the mid-body segment A3. To clearly analyze the relation between crawling speed and proleg lift during individual steps, the times of successive peaks in forward velocity were smoothed, as shown in Fig. 15a. The vertical displacement of A3 is highly correlated to the increase in horizontal velocity.

As A3 lifts, it moves forward with no phase delay. In contrast, the kinematic behavior for individual modules of the robot is similar to the findings in real caterpillars. Considering the position of A3, we analyzed module 4 of the robot. Fig. 15b shows the horizontal velocity varies in the swing phase and goes back to zero when the module switches to the stance phase. A peak forward rate emerges around the time when the displacement in the y-plane achieves the maximum value. In other words, the crawling pattern looks very similar as is illustrated in Fig. 15a, i.e., the horizontal velocity and the vertical displacement are in phase.

5.3 Efficient caterpillar-like locomotion

The efficiency of caterpillar-like locomotion was studied in two aspects. First, the step length $\Delta\lambda$ in one crawling cycle with respect to different amplitudes and phase differences was investigated. Considering the number of modules of the robot, only three groups of phase differences ($\pi/2$, $\pi/3$ and $\pi/4$) were tested. Second, the energy consumption in one complete step cycle was examined by means of the current-sense amplifiers (Maxim, MAX4173). The current is accumulated by sampling within an interval of *100ms*. The total energy consumption is thus a production of the voltage from a constant power supply, the accumulated current from the current-sense amplifiers, and the elapsed time. The experiment was repeated 5 times for every specific amplitude and phase difference, and the averaged data was saved for evaluation.

Fig. 16a shows the measurements of the step length per cycle. The step length increases with the growth of the amplitude, but not as expected as the theoretical values in Fig. 7b. This is because during the experiment, for the phase differences $\pi/2$, $\pi/3$ and $\pi/4$, the sliding phenomenon happens as the amplitude increases to *35°*, *30°* and *20°*, respectively. Meanwhile, due to torque limitation, the half wave loses its form during the propagation once the amplitude reaches a higher value. Fig. 16b shows the energy consumption the robot used during the experiment. The energy consumption increases almost linearly as the amplitude increases. Furthermore, with the decrease of the phase difference, the number of involved modules increases and thus the increment of the energy consumption rises rapidly.

In order to evaluate the locomotion efficiency of the caterpillar-like robot under different locomotion parameters, the ratio between the step length and the energy consumption is considered as the target of evaluation. Fig. 16c illustrates how the amplitude and the phase

difference affect the efficiency of caterpillar-like locomotion. On the one hand, the efficiency increases as the amplitude increases. However, its increment decreases gradually until the efficiency approaches a saturation stage. On the other hand, when the amplitude is small, e.g., $A \leq 20$, a smaller phase difference results in an overall higher efficiency. As the amplitude continues to increase, the efficiency for a smaller phase difference will enter the saturation stage ahead of the efficiency for other larger phase differences. The figure also shows the most efficient caterpillar-like locomotion occurs when the amplitude achieves around $35°$. Combined with Fig. 16a and 16b, although further increasing the amplitude increases the step length, the slippage and the torque issue counteract its effect, whereas the energy consumption keeps almost the same increasing speed. As a consequence, the efficiency declines once the amplitude exceeds $35°$.

From the results, we conclude that the proposed CPG model with asymmetric oscillation works well for realizing efficient caterpillar-like locomotion.

6 Conclusion

In this paper, we emphasize the analysis and design of an asymmetric oscillating mechanism for caterpillar-like locomotion. According to the behavior analysis of caterpillars in nature, two interesting properties, including an alternate switch between the swing phase and the stance phase and a phase lag among caterpillar's segments, are extracted. A hypothesis of asymmetric oscillation with a ratio of two is proposed and its stability for the generation and the propagation of the 'hump' body shape is thoroughly analyzed. A CPG model based on the Hopf oscillator is designed, in which the locomotive properties of caterpillars together with the hypothesis are well integrated. It guarantees that the caterpillar-like locomotion is stable and capable of online modulation. Through simulation and on-site experiments, including comparison with real caterpillars and energy evaluation, the effectiveness of the approach is verified in realizing efficient caterpillar-like locomotion.

There is still a long way to go before caterpillar-like robots can achieve the free movements that exist in natural environments. Real caterpillars move with a variety of reactive behaviors, which requires the use of additional sensory information. Currently, we are designing new robot modules with different types of sensors. Future research will focus on integrating sensory feedback into the system, towards the goal of adaptive caterpillar-like locomotion.

Acknowledgement

The research presented in this paper was partly supported by the Deutsche Forschungsgemeinschaft (DFG) (No. U-4-6-04-DFG-10-01).

References

[1] Carl G. Locomotion of limbless vertebrates: pattern and evolution. *Herpetologica*, 1986, **42**, 33-46.

[2] Hirose S, Yamada H. Snake-like robots. *Robotics & Automation Magazine*, 2009, 16, 88-98.

[3] González-Gómez J, Aguayo E, Boemo E. Locomotion of a modular worm-like robot using a FPGA-based embedded microblaze soft-processor. *Proceeding of the 7th International Conference on Climbing and Walking Robots*, Madrid, Spain, 2004, 869-878.

[4] Wang W, Wang K, Zhang H X, Zhang J W. Internal force compensating method for wall-climbing caterpillar robot. *Proceedings of the 2010 IEEE International Conference on Robotics and Automation*, Alaska, USA, 2010, 2817-2820.

[5] Cai Y, Bi S, Zheng L. Design and experiments of a robotic fish imitating cow-nosed ray. *Journal of Bionic Engineering*, 2010, **7**, 120-126.

[6] Hopkins J K, Spranklin B W, Gupta S K. A survey of snake-inspired robot designs. *Bioinspiration & Biomimetics*, 2009, **4**, 1-19.

[7] Yim M, Duff D, Roufas K. Polybot: a modular reconfigurable robot. *Proceeding of 2000 IEEE International Conference on Robotics and Automation*, San Francisco, USA, 2000, 514-520.

[8] Kurokawa H, Tomita K, Kamimura A, Kokaji S, HasuoT, Murata S. Distributed self-reconfiguration of M-TRAN III modular robotic system. *The International Journal of Robotics Research*, 2008, **27**, 373-386.

[9] Rus D, Vona M. Crystalline robots: self-reconfiguration with compressible unit modules. *Autonomous Robots*, 2001, **10**, 107-124.

[10] Hirose S. *Biologically inspired robots*. Oxford University Press, London, UK, 1993.

[11] Crespi A, Badertscher A, Guignard A, Ijspeert A J. Swimming and crawling with an amphibious snake robot. *Proceedings of the 2005 IEEE international conference on robotics and automation*, Barcelona, Spain, 2005 3024-3028.

[12] Yamada H, Hirose S. Development of practical 3-dimensional active cord mechanism ACM-R4. *Journal of Robotics and Mechatronics*, 2006, **18**, 305-311.

[13] Borenstein J, Hansen M, Borrell A. The OmniTread OT-4 serpentine robot–design and performance. *Journal of Field Robotics*, 2007, **24**, 601-621.

[14] Grillner S. Neurobiological bases of rhythmic motor acts in vertebrates. *Science*, 1985, **228**, 143-149.

[15] Ijspeert A J. Central pattern generators for locomotion control in animals and robots: a review. *Neural Networks*, 2008, **21**, 642-653.

[16] Chirikjian G, Burdick J. The kinematics of hyper-redundant robot locomotion. *IEEE Transactions on Robotics and Automation*, 1995, **11**, 781-793.

[17] Yim M. *Locomotion with unit-modular reconfigurable robot*. PhD thesis, Stanford, CA, USA, 1994.

[18] Li G Y, Zhang H X, Herrero-Carrón F, Hildre H P, Zhang J W. A novel mechanism for caterpillar-like locomotion using asymmetric oscillation. *Proceedings of the 2011 IEEE International Conference on Advanced Intelligent Mechatronics*, Budapest, Hungary, 2011, 164-169.

[19] Brackenbury J. Caterpillar kinematics. *Nature*, 1997, **390**, 453-453.

[20] Brackenbury J. Fast locomotion in caterpillars. *Journal of Insect Physiology*, 1997, **45**, 525-533.

[21] Trimmer B A, Issberner J. Kinematics of soft-bodied, legged locomotion in manduca sexta larvae. *Biological Bulletin*, 2007, **212**, 130-142.

[22] Lin H T, Trimmer B A. The substrate as a skeleton: ground reaction forces from a soft-bodied legged animal. *Journal of experimental biology*, 2010, **213**, 1133-1142.

[23] Trivedi D, Rahn C D, Kier W M, Walker I D. Soft robotics: Biological inspiration, state of the art, and future research. *Applied Bionics and Biomechanics*, 2008, **5**, 99-117.

[24] Marbach D, Ijspeert A J. Online Optimization of Modular Robot Locomotion. *Proceedings of the 2005 IEEE International Conference on Mechatronics and Automation*, Niagara Falls, Canada, 2005, 248-253.

[25] Smith R, Open dynamics engine, http://www.ode.org/.

[26] Zhang H, Gonzalez-Gomez J, Xie Z, Cheng S, Zhang J. Development of a low-cost flexible modular robot GZ-I. *Proceeding of the 2008 IEEE/ASME International Conference on Advanced Intelligent Mechatronics*, Xian, China, 2008, 223-228.

[27] Casey T M. Energetics of caterpillar locomotion: biomechanical constraints of a hydraulic skeleton. *Science* 1991, **252**, 112–114.

[28] Van Griethuijsen L I, Trimmer B A. Kinematics of horizontal and vertical caterpillar crawling. *Journal of Experimental Biology* 2009, **212**, 1455-1462.

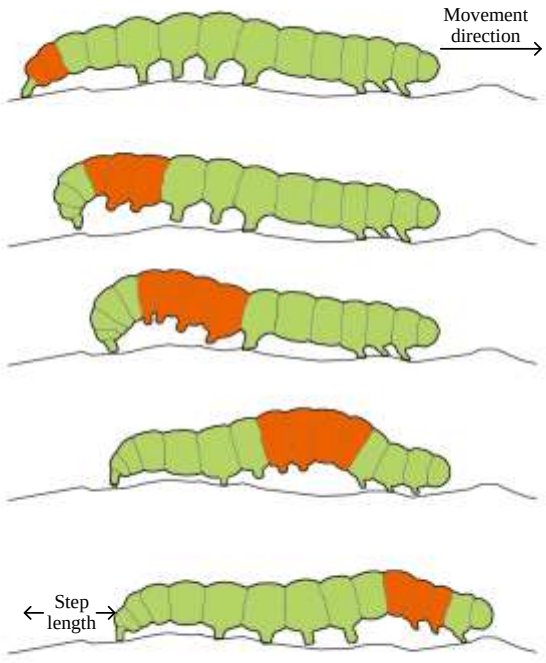

Fig. 1 Caterpillar forward locomotion, adopted from [20].

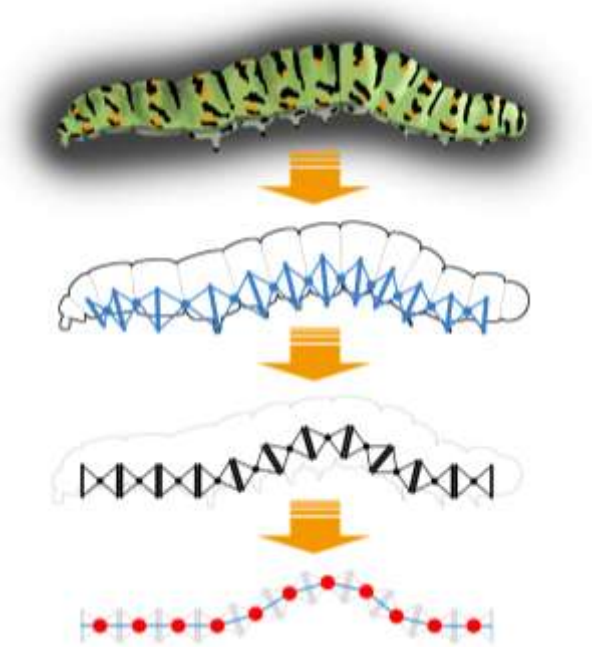

Fig. 2 Morphological mapping from the caterpillar to the modular robot to the skeleton model.

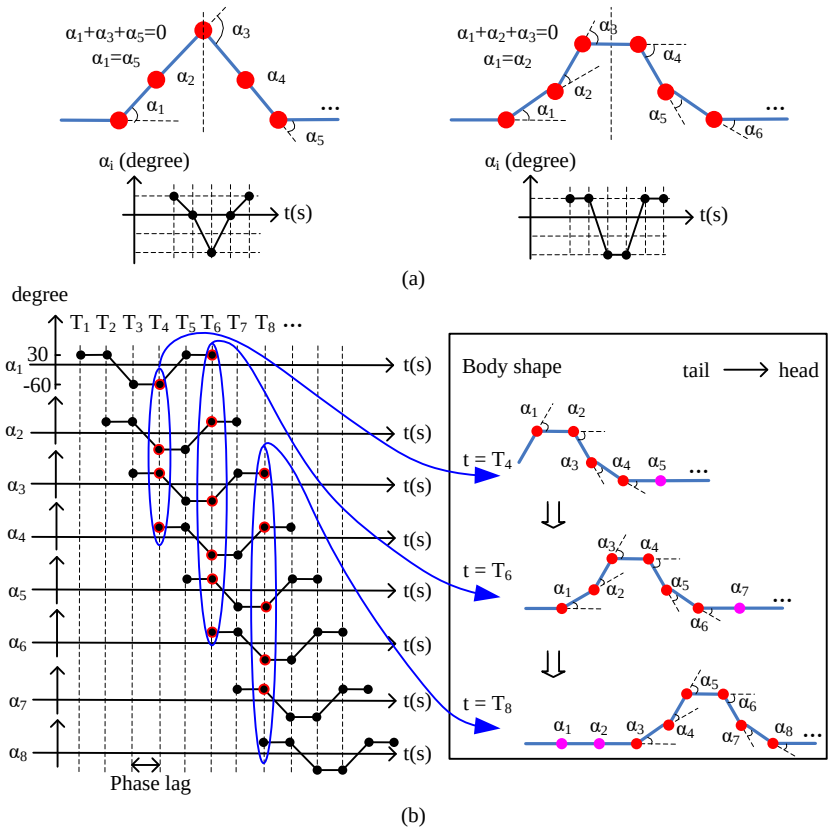

Fig. 3 Discrete body shape analysis. (a) Two types of body shape in the half wave as well as their angle variation over discrete time. (b) An example of half wave generation and propagation with respect to discrete time sequence.

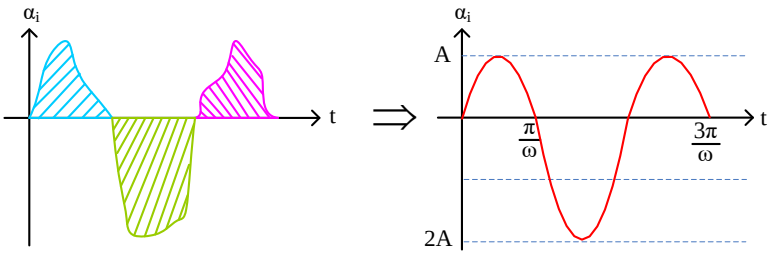

Fig. 4 Hypothesis of continuous angle variation in the swing phase.

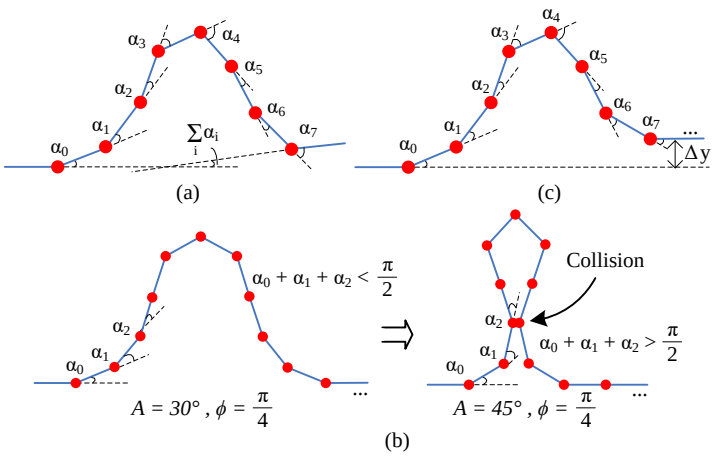

Fig. 5 Continuous body shape analysis. (a) Joint analysis. (b) Collision analysis. (c) Vertical displacement analysis.

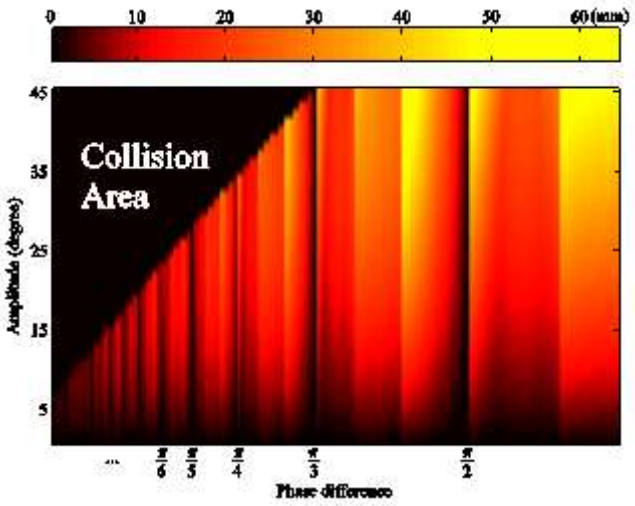

Fig. 6 The vertical displacement with respect to the amplitude and the phase difference.

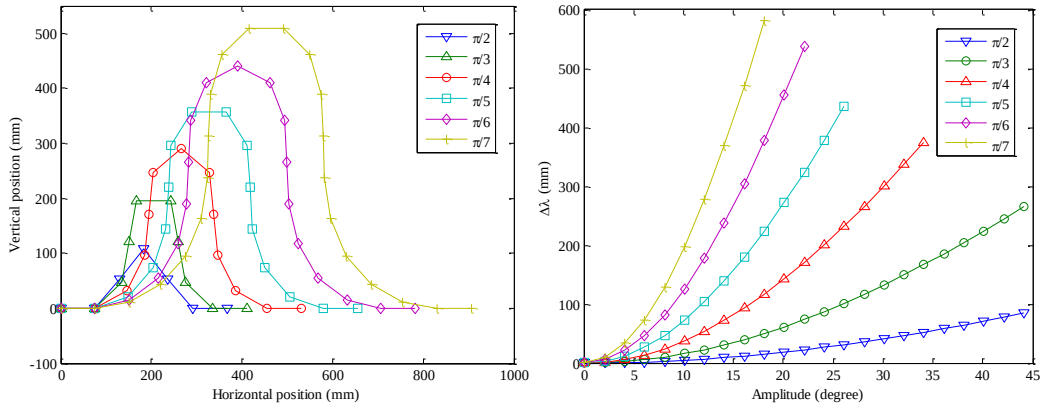

(a) (b)

Fig. 7 Horizontal displacement analysis. (a) The body arcs with respect to a series of phase differences. (b) Horizontal displacement per step cycle with respect to the amplitude and the phase difference.

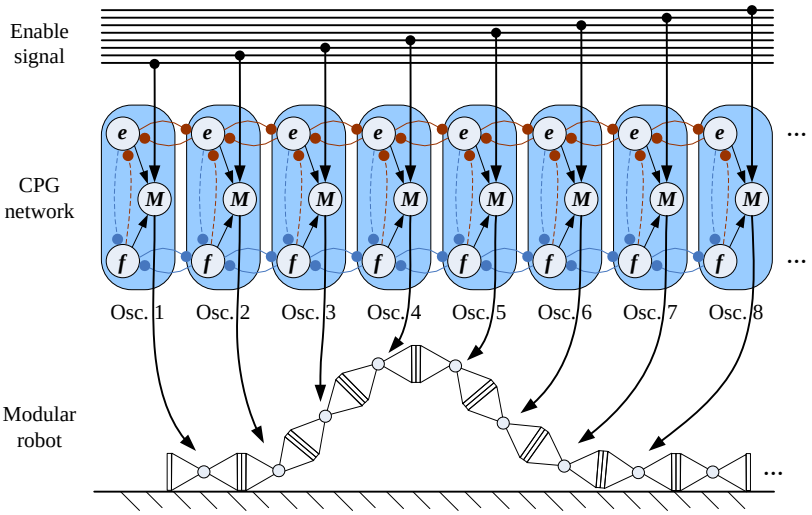

Fig. 8 The CPG-based control architecture.

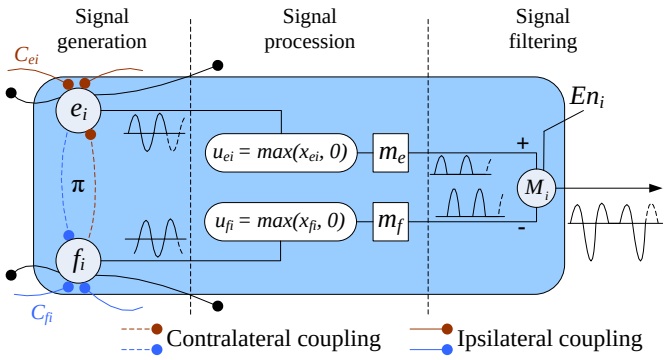

Fig. 9 The detailed oscillator model.

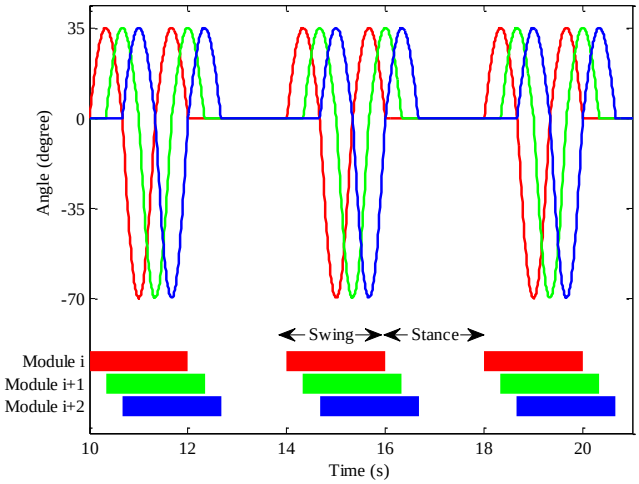

Fig. 10 The output of three oscillators in the CPG model.

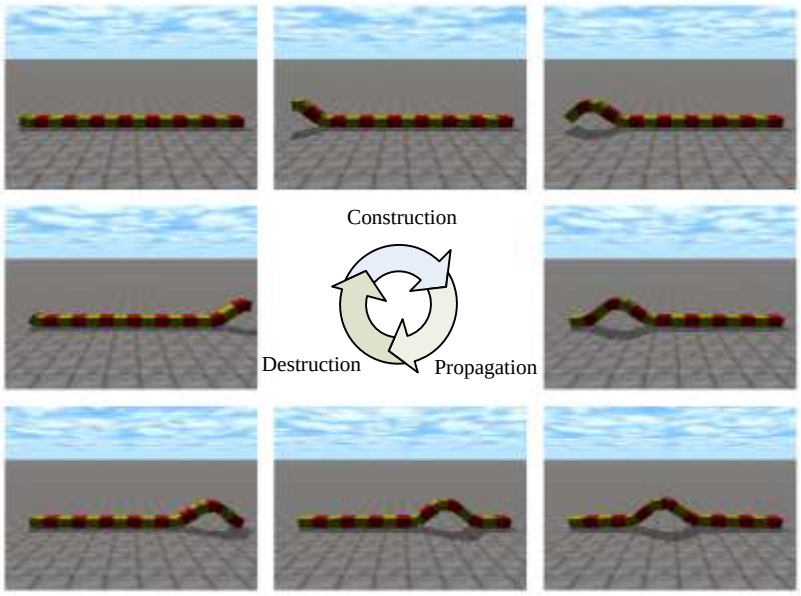

Fig. 11 Simulation of caterpillar-like locomotion in one step cycle.

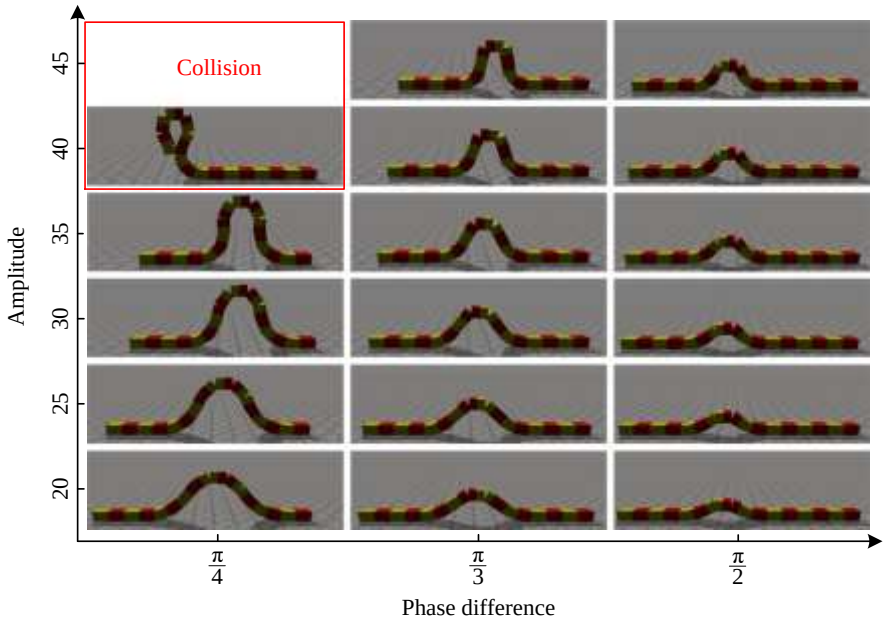

Fig. 12 Body shape variation with respect to the amplitude and the phase difference.

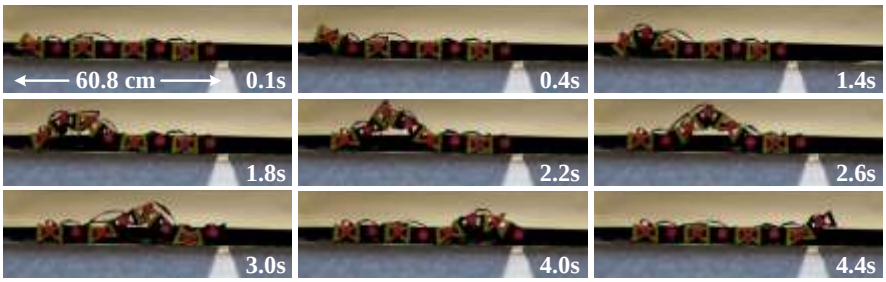

Fig. 13 On-site experiment.

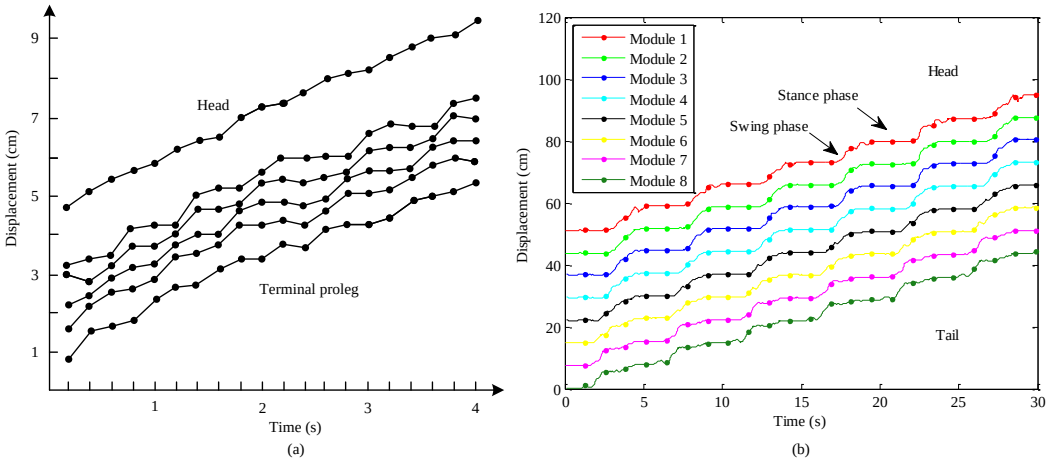

Fig. 14 The horizontal displacement comparison. (a) Real caterpillar data, adopted from [27]. (b) On-site experimental data.

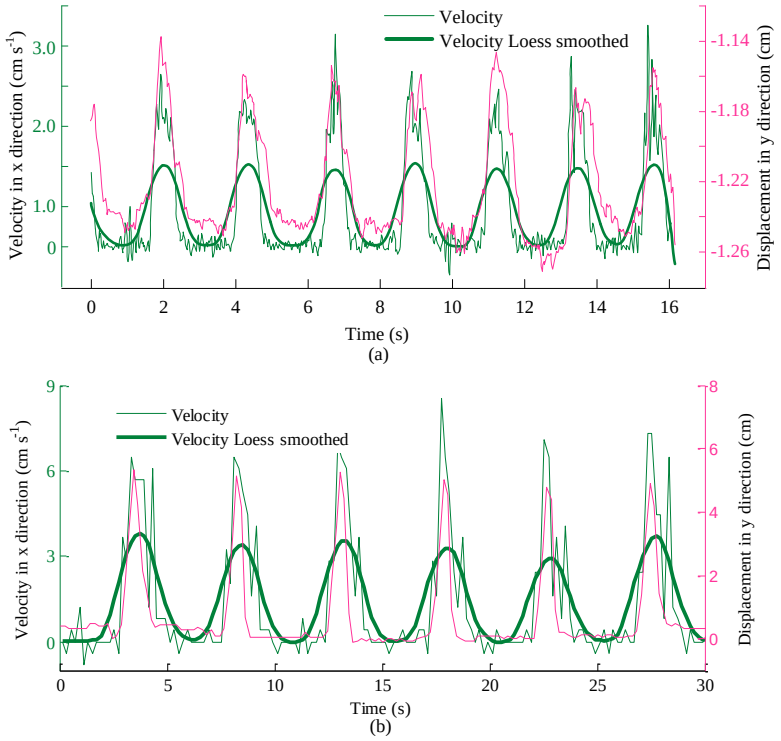

Fig. 15 Velocity in the x-plane and displacement in the y-plane versus time. (a) Data for A3 of real caterpillar, adopted from [28]. (b) Data for module 4 of the robot.

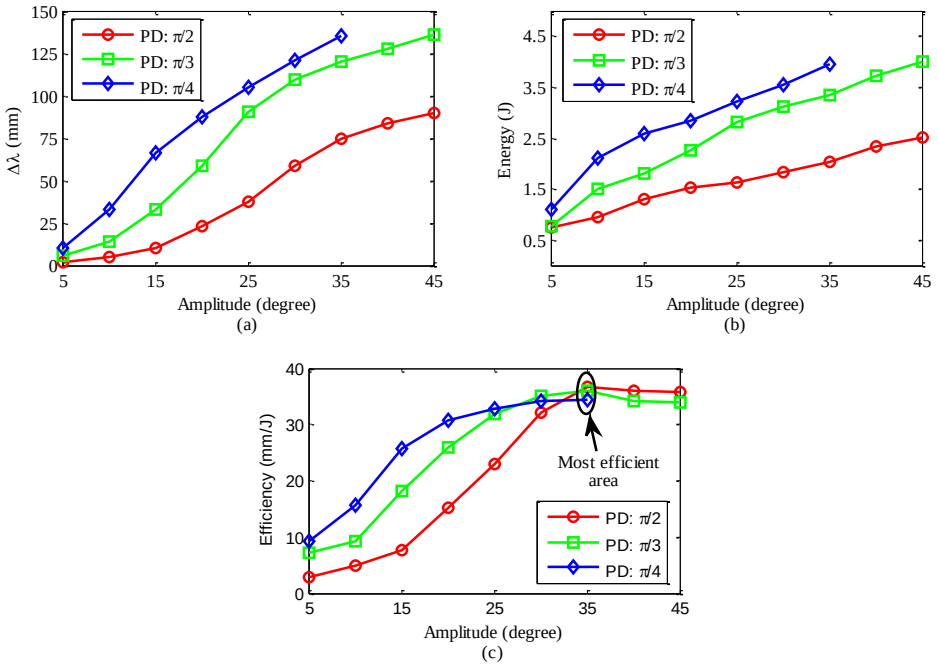

Fig. 16 Measured data. (a) The step length Δλ. (b) The energy consumption. (c) Efficiency of caterpillar-like locomotion.

Table 1 Parameters of the CPG network

Symbol	Value	Description
ω	$(0, 2\pi]$	Frequency
A	$(0, 45]$	Amplitude
ϕ	π/n, $(n \geq 2)$	Phase difference
w	$(0, 2]$	Coupling weight
m_e, m_f	1, 2	Oscillating ratio

Table 2 Specification of the GZ-I module

Component	Parameters	Value
Module	Size	76 × 52 × 52 *mm*
	Weight	150 *g*
RC servo motor (Futaba s3003)	Rotate speed	< 1.45 *rad/s*
	Torque	< 0.314 *Nm*

Fig. 1 Caterpillar forward locomotion, adopted from [20].

Fig. 2 Morphological mapping from the caterpillar to the modular robot to the skeleton model.

Fig. 3 Discrete body shape analysis. (a) Two types of body shape in the half wave as well as their angle variation over discrete time. (b) An example of half wave generation and propagation with respect to discrete time sequence.

Fig. 4 Hypothesis of continuous angle variation in the swing phase.

Fig. 5 Continuous body shape analysis. (a) Joint analysis. (b) Collision analysis. (c) Vertical displacement analysis.

Fig. 6 The vertical displacement with respect to the amplitude and the phase difference.

Fig. 7 Horizontal displacement analysis. (a) The body arcs with respect to a series of phase differences. (b) Horizontal displacement per step cycle with respect to the amplitude and the phase difference.

Fig. 8 The CPG-based control architecture.

Fig. 9 The detailed oscillator model.

Fig. 10 The output of three oscillators in the CPG model.

Fig. 11 Simulation of caterpillar-like locomotion in one step cycle.

Fig. 12 Body shape variation with respect to the amplitude and the phase difference.

Fig. 13 On-site experiment.

Fig. 14 The horizontal displacement comparison. (a) Real caterpillar data, adopted from [27]. (b) On-site experimental data.

Fig. 15 Velocity in the x-plane and displacement in the y-plane versus time. (a) Data for A3 of real caterpillar, adopted from [28]. (b) Data for module 4 of the robot.

Fig. 16 Measured data. (a) The step length $\Delta\lambda$. (b) The energy consumption. (c) Efficiency of caterpillar-like locomotion.